Land-sea Thermal Contrast in Relation With Summer Monsoon Onset Over the Chao Phraya River Basin

Tomohito J. Yamada
https://orcid.org/0000-0002-0031-4283
Sourabh Shrivastava (sourabh.vds@gmail.com)
NCMRWF
Ryosuke Kato

Research Article

Keywords: Asian summer monsoon onset, Tibet, Bay of Bengal, MJO, Indochina Peninsula

Posted Date: January 10th, 2022

DOI: https://doi.org/10.21203/rs.3.rs-1218001/v1

Abstract

An earlier onset of the Southeast Asian summer monsoon (SAM) was observed over the Chao Phraya River basin in Thailand using Thai Meteorological Department (TMD)-derived high-resolution merged rainfall from 1981 to 2016. As the SAM is precipitous, its variability depends on many local and global factors, such as thermal conditions over the Bay of Bengal (BoB) and Tibetan Plateau (TbT). Despite tremendous studies in the past, the role of thermal heat contrast over SAM is still not fully understood. Using the observation and reanalysis datasets, it was found that the absolute value of total heat over the BoB was higher. However, the interannual variability in total heat is higher over the TbT. Significant changes in surface temperature (±1.5°C), air thickness (±20 meters) and geopotential height found over the TbT were associated with early (late) SAM onset. The results also suggested that the significant changes in air thickness were influenced by the surface temperature difference over the TbT, and the changes in the integrated apparent heat source and integrated apparent moisture sink were up to ± 100 $Wm^{-2,}$ which resulted in stronger (weaker) convective activities over the BoB and mainland of the Indochina Peninsula during early (late) SAM onset. At the intraseasonal timescale, the instance MJO found over the Indian Ocean and Western Hemisphere at 4 to 10 days span during early SAM onset. An opposite scenario is found for a late SAM onset years with MJO location over Western Pacific and Maritime continent.

Introduction

Thailand receives approximately 80% or more of its yearly total rainfall between May and October (Thai Meteorological Department (TMD), 2021) during the South Asian summer monsoon (SAM). However, the variability of the SAM onset has been seen as a topic of concern (*Zhou et al.* 2019). The reason behind this concern is that the production of rice highly depends on the condition of the SAM and its onset, and it also affects more than 69.6 million people in Thailand (The World Bank, 2019), especially over the Chao Phraya River basin (CPB), which covers an area of approximately 30% (157,925 km^2) of the mainland in Thailand. Moreover, it also contributes to a major part of the Thai GDP.

The characteristics of SAM onset have been extensively discussed in previous studies (Zhang et al. 2002; Takahashi & Yasunari, 2006; Ding, 2007; Kuraji and Arthorn, 2011; Kajikawa *et al.* 2012; Nguyen-Le, 2015; Shrivastava et al., 2017; Tanaka *et al.* 2019). By using the rainfall index for 1951 to 1996, Zhang et al. (2002) defined the mean onset date over the central Indochina Peninsula (ICP) as approximately the 26^{th} pentad of the year. However, the variability in SAM onset is also a topic of concern. For example, Kajikawa *et al.* (2012) found that the SAM became earlier over the ICP between 1994 and 2008 and 1979 and 1993 by using CPC merged analysis of precipitation (CMAP) at a 2.5 x 2.5 degree spatial resolution. Minoura *et al.* (2003) also discussed the mechanism of SAM onset and characterized ICP by a relatively slow onset by using European Centre for Medium-Range Weather Forecasts (ECMWF) reanalysis (ERA) data with a spatial resolution of 2.5 x 2.5 from 1982 to 1993. In ground observations, the earlier trend in SAM onset was also found by Kuraji and Arthorn (2011) and Tanaka *et al.* (2019) in the Mae Chaem watershed (few observation points) only over the ICP. In recent decades, long-term high-resolution gauge

rainfall data over the ICP have become available for research purposes. Therefore, our first question is whether the SAM onset has still been getting earlier in recent decades or whether it has changed.

In the past, extensive efforts were made to determine the relationship between SAM onset and the various contributing factors (for example, Minoura *et al.* 2003; Kiguchi *et al.* 2016). Takahashi and Yasunari (2006) constructed the climatological mean values of rainfall over 50 years and showed a distinct climatological monsoon break occurring at approximately the 33rd pentad over the ICP with a drastic change in large-scale monsoon circulation in the seasonal march. Kiguchi *et al.* (2016) analyzed premonsoon rainfall to identify its relationship with SAM onset. However, no clear relationship has been identified. Minoura *et al.* (2003) also discussed the mechanism of SAM onset and determined that the Indian summer monsoon (ISM) onset is relatively slower than the SAM onset and suggested that the ISM and SAM onset are distinguished from each other. Now, the question is whether global teleconnections affect SAM onset over the ICP. Takahashi and Yasunari (2006) identified a trough over the Bay of Bengal (BoB) during early SAM onset; at the same time, weak southwesterlies also appeared over the eastern Indian Ocean and after high precipitation was recorded over the ICP. Many efforts in the past have also focused on the SAM onset measured by the El Nino-Southern Oscillation (ENSO) and Indian Ocean dipole (IOD) and documented the relationship between the early/late onset of the SAM and large-scale variability modes (Wu & Wang, 2000; Wang et al., 2001; Ding, 2007). Wu and Wang (2000) also show the link between ENSO and SAM onset. However, their research indicated that the physical processes in the land and ocean areas are crucially responsible for reduced land-ocean thermal contrast. Moreover, at the intraseasonal scale, the Madden-Julian oscillation (MJO) could also affect the SAM onset (Chi *et al.* 2015). The MJO is one of the dominant modes of intraseasonal variability in the tropics (Madden and Julian, 1972). The eastward-moving MJO is associated with deep convection and circulation from eastern Africa, the Indian Ocean, and the Maritime Continent to the Western Pacific (Madden and Julian, 1971; Madden and Julian, 1972). When the MJO moves to the eastern Indian Ocean and the western Indian Ocean, it has an impact on the SAM onset (Chi *et al.* 2015). Nevertheless, the MJO influenced by the thermal conditions over the Indian Ocean is not very clear because of the late (early) SAM. Here, our concern is that the relationship of the SAM with local factors is not very clear. Therefore, our next question is whether the intensity and position of the MJO can influence SAM onset.

The heat contrast between the Asian landmass and the tropical Indian Ocean is very important for the advanced (weakening) SAM onset (Kajikawa *et al.* 2012). The relationship between sea surface temperature (SST) over the Bay of Bengal (BoB) and rainfall over the ICP was not clarified (Kanae *et al.* 2002). Therefore, some studies have focused on the effect of the land–sea thermal contrast on the SAM (Wu and Wang, 2000; Nguyen-Le *et al.* 2015). For the establishment of the SAM, the TbT is an elevated heat source (Yanai *et al.* 1992; Abe *et al.* 2013), and it has a great impact on the transition of SAM rainfall (Wang *et al.* 2001; Sato and Kimura, 2007). Yanai *et al.* (1992) revealed that the increase in temperature over the eastern Plateau during the SAM onset was mainly because of diabatic heating. Minoura *et al.* (2003) provided strong evidence between thermal contrast and SAM onset over the ICP. Zhang *et al.* (2017) found a significant thermal difference through the atmospheric heat source, and their results

suggested that the SAM onset time lags behind the time of thermal change. Moreover, the importance of sensible heat flux in the western Plateau and the latent heat release over eastern India and the adjoining region was very well suggested by Flohn (1957). After analyzing the observation data, Xu and Chan (2001) found that the sensible and latent heat fluxes both dominate the thermal condition over the TbT. In the past, to understand the apparent heat source (Q1) and/or apparent moisture sink (Q2) and its link with large-scale atmospheric circulation, many studies have been performed (Yanai *et al.* 1973; Schumacher *et al.* 2008; Xing *et al.* 2016). Despite advances, many important and basic questions remain unanswered, such as how the thermal conditions over the western TbT influence and interact with the SAM onset and how the apparent heat source and apparent moisture sink behave during SAM onset over the BoB and ICP. Therefore, an effort has been made to explain the possible mechanism of early (late) SAM onset over the CPB. It is already known that the SAM onset over the CPB starts in May. Here, we focus on the first three pentads of May in our study (details shown in the data used section).

The remainder of this paper is organized as follows. In Section 2, we describe the data and methods used in this study. In Section 3, the results and discussion are presented. The conclusion of the study is provided in Section 4.

Data And Methods

Observational and reanalysis data

We mainly used the Thai Meteorological Department (TMD)-derived high-resolution merged rainfall with 0.05^{o} x 0.05^{o} spatial resolution to investigate the climatology and fraction of rainfall corresponding to early- and late-onset years and plotted pentad rainfall over the ICP between 1981 and 2016. To investigate the temperature variability over East Asia, we used the gauge-based high-quality temperature dataset APHRODITE V1808 (Yasutomi *et al.* 2011), specifically the monsoon Asia version of APHRODITE with a spatial resolution of 0.5°×0.5° from 1979-2015. For SST, the Optimum Interpolation SST (OISST) of the National Centers for Environmental Information (NCEI)/National Oceanic and Atmospheric Administration (NOAA) has a 0.25° × 0.25° spatial resolution from 1981 to 2016 (Reynolds *et al.* 2007). Three-dimensional atmospheric data were used from The Modern Era Retrospective analysis for Research and Applications, Version 2 (MERRA2) for 1981 to 2016. The 3 hourly averaged data for air temperature, wind circulation, omega, relative humidity, and geopotential height were downloaded (GMAO, 2021). MERRA2 was developed with the Goddard Earth Observing System (GEOS-5.12.4) atmospheric data assimilation system (ADAS) with a spatial resolution of 0.5° x 0.625° (Gelaro *et al.* 2017). We used MERRA-2 because in MERRA, the horizontal discretization of the model was computed on a latitude–longitude grid, whereas MERRA-2 uses a cubed-sphere grid; plus, it controls for the variable for moisture used in recent versions of GSI, and MERRA-2 differs from the one used in MERRA. In comparison with the MERRA system, the background error statistics for the MERRA-2 system exhibit smaller standard deviations for many variables. However, both larger and smaller correlations depend on the variable, latitude, and vertical level. Moreover, MERRA included no new satellite observation sources after the introduction of *NOAA-18* in 2005. MERRA-2, in contrast, includes numerous additional satellite

observations both before and after this time (Gelaro *et al.* 2017). The real-time multivariate MJO indices (RMM1 and RMM2) of Wheeler and Hendon (2004) were used to define the various phases of MJO (RMM, 2021).

Methodology

Definition of SAM onset date and early (late) years

Pentad (5-day) mean rainfall and other atmospheric variables were constructed for the 36-year period. The methodology and definition for the estimation of SAM onset adopted from Wang and Ho (2002) over 98°E – 103°E and 13°N – 20°N (CPB), where the definition is that the relative rainfall rate exceeds 5 mm/day after deducting the January mean and occurs during the boreal summer (May-September), is defined as the onset pentad. In a previous study, Zhang et al. (2002) found that most early (late) years are similar to Wang and Ho's (2002) definition. Therefore, in further analysis, sample sizes of the top 9 early (1986, 1988, 1994, 1995, 1999, 2000, 2001, 2002 and 2007) and 9 late (1983, 1987, 1991, 1992, 1993, 1997, 2010, 2013, and 2015) onset years were used.

Here, we choose the first three pentad rainfall events in May because Figure 1(a) shows that the CPB receives approximately 50% or more of the rainfall events in the first three pentads in May. In early (late) onset, the fraction of the rainfall amount was 60% (40%) (Figure 1b-1c). Moreover, Figure 1c shows the daily mean rainfall and the difference in rainfall amount. This difference occurs before the first three pentads of May, and after the 3rd pentad, the difference becomes negligible between all three categories. Therefore, based on our analysis, we found that the first three pentads in May are reasonable to define the early and late onset years.

Apparent heat source (Q1) and apparent moisture sink (Q2)

We calculate the atmospheric Q1 and Q2 based on the thermodynamic equation. The equations used are as follows (Yanai *et al.* 1973):

$$Q_1 = c_p \frac{\partial T}{\partial t} - c_p(\omega\sigma - \mathbb{V} \cdot \nabla \mathrm{T}) \ , \qquad (1)$$

$$Q_2 = -\left(L \frac{\partial q}{\partial t} + L\mathbb{V} \cdot \nabla q + L\omega \frac{\partial q}{\partial p}\right) .$$

Here, the variables are the air temperature (T), time (t), horizontal wind vector (V), vertical wind vector (ω), specific heat at constant pressure (Cp), latent heat of condensation (L), specific humidity (q), static stability (σ), pressure (p) and the horizontal gradient operator (∇).

The vertically integrated forms of Q1 and Q2 can be written as follows:

$$< Q1 > \approx LP + S + < Q_R >, \quad (3)$$

$$< Q2 > \approx L(P - E), \quad (4)$$

where Q_R is the radiative heating rate and P, S and E are the precipitation rate, the sensible heat flux and the evaporation rate per unit area at the surface, respectively (Yanai *et al.* 1973, 1992).

$$<> = \frac{1}{g}\int_{pt}^{pb}(\ )\ dp\ . \quad (5)$$

where pt (300 hPa) is the pressure at the top pressure level and pb (1000 hPa) is the pressure at the surface.

The Madden-Julian oscillation (MJO)

The MJO is known as a 30-to-60-day oscillation or intraseasonal oscillation. The MJO can modulate the timing and strength of the SAM (Jones and Carvalho, 2002). We choose the approximate location of the MJO (David et al., 2004) mentioned in Figure 2, and the MJO travels east at 4-10 days/phase. Therefore, we chose a 10-day period to check the intensity and location of the MJO during SAM onset.

Results

Changes in SAM onset and climatological features of SAM onset

Towards the first research question, in this section, the difference in the SAM onset pentad between 1999-2016 and 1981-1998 over each grid of northern Thailand is plotted. In Figure 1d, the results suggested that the SAM onset occurred earlier (approximately two to four pentads) in the last ~2 decades over the CPB. The results are different from older studies, such as Kajikawa *et al.* (2012), because they clearly show that the frequency of early onset has increased in recent decades.

To understand the climatological features of surface and atmospheric variables during SAM onset. In this section, wind vectors (850 hPa), specific humidity (850 hPa), temperature (land and ocean) and geopotential height (500 hPa) are averaged over the 36-year period from 1981 to 2016. In Figure S1(a), at 850 hPa, the prominent pattern of wind systems is the cross-equatorial flow caused by the southwesterlies in the first three pentads of May, and the southwesterlies also cross the ICP and move toward the South China Sea. The sets of northwesterlies coming from northwest India and the adjoining region to the ICP are also dominant during the onset period, especially over the northern BoB. In Figure S1(b), the specific humidity (g/kg) over the BoB (<10 g/kg) is lower than the ICP (>10 g/kg) identified. In Figure S1(c), a warmer Indochina Peninsula (>28 °C) than the BoB (>25 °C) is seen. Moreover, the TbT, with a temperature < 10 °C, is found in warmer northwestern India, Pakistan and Afghanistan regions. The 500 hPa geopotential height exceeding 5850 gpm over the BoB and > 5750 gpm over the TbT and trough over the ICP are shown in Figure S1(d). Figure 3a shows the climatology of air thickness that was

calculated by the height between 200 hPa minus 500 hPa. In this plot, air thickness is more than 6800 meters over the BoB, which is much higher than air thickness over the TbT. It clearly shows that the air thickness increased over the BoB and associated region, including the ICP, during the onset period.

Associated signals and climatology versus early (late) SAM onset

To identify the associated signals caused by the change in SAM onset over the CPB, the air thickness anomalies are plotted for the first three pentads of May because in the monsoon region, the atmospheric thickness is an essential parameter between 200 and 500 hPa (Li and Yanai, 1996; Kajikawa *et al.* 2012). In Figure 3b, highly significant changes in air thickness are seen over the western TbT, Northwest India, Pakistan, the BoB and ICP. However, air thickness is much higher over the TbT than over the BoB, and this difference is more than 30 meters. This result indicates that air thickness over the TbT influences early SAM onset. On the other hand, air thickness becomes thinner over central India, the TbT and the BoB, but air thickness is much thinner over central India and the BoB than over the TbT. It also indicates that the local factor in the BoB influences the onset. To go into more detail, the longitudinal profile of the heat contrast between land and ocean is plotted for each pentad of the year (shown for the 27^{th} to 37^{th}). Figure 4a shows the climatological average, that is, the average for the early and late SAM onset pentads of the year when the thermal contrast reaches zero between 27.5–N - 37.5°N (land) and 5–N - 15°N (ocean). We have found that the large shift in thermal heat contrast at 98°E to 100°E over the ICP in the early SAM onset and process occurs earlier by 3 pentads with a standard deviation ±4. In the case of the late SAM onset, the delay in the whole process takes approximately one pentad versus the climatology with a standard deviation of ± 2. These results indicated that land (TbT) was the dominant factor causing early SAM onset, followed by the BoB. In Figure 4b-c, the difference in the thermal contrast between early (late) years against climatology is plotted. In early onset, 90% significant thicker anomalies were found in the upper troposphere along with the western TbT between 25 and 28 pentads (May), associated with the positive (negative) changes more than ±1.5 -2.0 °C in surface temperature anomalies (Yanai et al., 1992) shown in Figure 5e-5f over the western TbT and the nearest region over the CPB. It is the time when the ICP receives the first spell of rainfall (Zhang et al. 2002), but it seems that if air thickness increases (decreases) between 60 and 80 degrees east (over western TbT) by ± 20 meters, it could affect the SAM onset. However, during the full monsoon period (May to October), large changes in air thickness are not noticed. At a geopotential height of 500 hPa (Figure 5g), positive anomalies found over the western TbT and northwestern India were associated with Pakistan and Afghanistan in early years, and negative anomalies were found over the BoB. In Figure 5g, the increased 500 hPa geopotential height over the TbT during the early onset was related to warming of the upper troposphere. This could be a possible reason for the strong northwesterlies toward the ICP in early years. In contrast (Figure 5h), the opposite pattern was identified in late onset years, where the western and central TbT have negative anomalies and the Arabian Sea, BoB and South China Sea have positive anomalies of 500 hPa geopotential height caused by a delay in SAM onset over the CPB.

From the above statement, it is clear that the thermal conditions are the opposite of those of the BoB and TbT. Therefore, it is very important to understand the role of other atmospheric and surface patterns as well. In Figure 5e-f, cold (warm) surface temperatures and SST anomalies are found over the ICP and BoB in early (late) onset years, it was also discussed by the (Chengfeng & Michio, 1996; Xing et al., 2016). The dipole (temperature anomaly over the TbT and BoB) pattern shows favorable climatic conditions and high pressure over northwestern India, Pakistan, and western TbT in early onset; it seems that a low-pressure system formed over the BoB with intense westerlies causing early onset. Cyclonic (anticyclonic) circulation in an early (late) onset year north of the BoB in the lower troposphere is present (Xing *et al.* 2016). Moreover, in Figure 5a, the strong energetic southwesterly monsoon approached the Indochina Peninsula and transported moisture from the ocean to land, which caused an increase in the specific humidity over the ICP in the early years (Figure 5c). In contrast, weaker winds (Figure 5b) and less specific humidity (Figure 5d) were found at late SAM onset.

After analysis of the thermal contrast and other atmospheric variables, <Q1> Wm^{-2} and <Q2> Wm^{-2} are averaged for the period of 1981-2016. Climatologically (Figure 6a-6b), the TbT and mainland ICP became heat sources during SAM onset compared to the ocean (Taylor et al., 2003). In Figure 6c-f, anomalies of <Q1> and <Q2> are investigated. In Figure 6c and 6d, anomalous increases in both <Q1> and <Q2> over mainland ICP are noticed in early SAM onset years that exceed 80 Wm^{-2} of <Q1> and <Q2>. The strong convection caused by southwesterlies wind was pushed by a strong MJO (Figure 7) and its position over the Indian Ocean and Maritime continent. The dominant position of the MJO during early SAM onset is in phases 1, 2, 3 and 4 (75% of the total early onset events). However, in the late SAM onset year, significant changes in <Q1> and <Q2> are noticed over the BoB (Figure 6e-6f). It also reflects the anomalous activities caused by late SAM onset; one is that the decreased latent heat leads to a reduction in specific humidity and weaker low-level winds, all of which are caused by the weak MJO and its position (Figure 7) during the late SAM onset. Here, only 2 events (15%) of the MJO were observed over the Indian Ocean and Maritime Continent. Moreover, of the two events, one event was a weak MJO. The reason behind this is that when the MJO stays in phases 1, 2, 3 and 4, it increases the convective activities over the ICP, as shown in Figure 1, and when it moves toward the east and crosses the Maritime Continent, then it may suppress convection over the ICP because of increased upward motion over the western Pacific.

Conclusion

In recent decades, earlier SAM onset has been noticed over the CPB by analyzing TMD rainfall. We have described the cause of the change in SAM onset over the CPB. The major findings in this work are as follows. First, in association with the early (late) onset, warmer (colder) surface conditions (±1.5 °C or more) over the western Tibetan Plateau and adjacent regions were detected. Anomalous changes (± 20 meters) in air thickness along with TbT were noticed during the first three pentads of May in early (late) onset caused by rising (decreasing) temperatures. However, in climatology, air thickness is higher over the BoB, but the changes in air thickness are higher over the TbT than over the BoB. During onset, TbT becomes a heat source, and in the investigation of <Q1> and <Q2>, positive (more than 150 W m^{-2})

changes were identified over the BoB, with stronger convective activities associated with the intense MJO in early SAM onset. Strong MJO position over Indian Ocean and Maritime continent clearly shows the increase in stormy conditions. It has seen that the years with warmer condition over TbT caused for initiation of stronger MJO. This MJO also spent around 4 to 10 days (in figure 7a) over Indian Ocean that caused for stormy conditions leads to an early SAM onset. In contrast, negative (approximately -100 W m^{-2}) anomalies in the late onset year were found, caused by a weaker southwesterlies over BoB. As the southwesterlies are weaker, the transport of moisture is over ICP is also very less, on the top of that the instead of heat source ICP gets cooler and the conditions are not in favor for SAM onset. In conclusion, thermal conditions over the TbT are dominant over early SAM onset but, because of several other reasons such as the weaker southwesterlies and low specific humidity over the BoB and cooler ICP suppress SAM onset.

Declarations

ACKNOWLEDGMENTS

This study was supported by the Ministry of Education, Culture, Sports, Science and Technology of Japan (MEXT) under the Research Program for Enhancing Integrated Climate Models, Theme C “Integrated Climate Change Prediction” JPMXD0717935561 and JSPS KAKENHI grant No. 19H02241, 19H00963. The Japan Science and Technology Agency/Japan International Cooperation Agency, and the Science and Technology Research Partnership for Sustainable Development (JST/JICA, SATREPS).

AUTHOR DECLERATION:

FUNDING:

This study was supported by the Ministry of Education, Culture, Sports, Science and Technology of Japan (MEXT) under the Research Program for Enhancing Integrated Climate Models, Theme C “Integrated Climate Change Prediction” JPMXD0717935561 and JSPS KAKENHI grant No. 19H02241, 19H00963. The Japan Science and Technology Agency/Japan International Cooperation Agency, and the Science and Technology Research Partnership for Sustainable Development (JST/JICA, SATREPS).

CONFLICT OF INTREST:

This research is purely original and there is no conflict of interest.

ETHICS:

This research is purely original and this research does not harm to the society or any individual knowingly and unknowingly.

CONSENT TO PARTICIPATE:

Informed consent was obtained from all individual participants included in this study.

DATA AVAILABILITY:

The rainfall datasets analysed during the current study are not publicly available. However, the data shall be requested to the Thai Meteorological Department (TMD).

Other datasets are publicly available such as surface temperature is from APHRODITE V1808 (Yasutomi *et al.* 2011), OISST is from NOAA (Reynolds *et al.* 2007), MERRA2 is from https://gmao.gsfc.nasa.gov/ (Gelaro *et al.* 2017), RMM is from Wheeler and Hendon (2004), and Figure 2 is from https://www.climate.gov/ with credit to Fiona Marton.

CODE AVAILABILITY:

All codes are developed using Python 3.6 except the <Q1> and <Q2> calculation the code is downloaded from the NCL library https://www.ncl.ucar.edu/.

AUTHOR CONTRIBUTION:

In this study, the research question and funding are raised by Dr. Tomohito J. Yamada, the data analysis and writing are done by Dr. Sourabh Shrivastava, and Mr. Kato helped for data collection.

References

Abe M, Hori M, Yasunari T, Kitoh A (2013) Effects of the Tibetan Plateau on the onsetof the summer monsoon in South Asia: The role of the air-sea interaction. *Journal of Geophysical Research: Atmospheres* **118**: 1760–1776. DOI: 10.1002/jgrd.50210.

Chengfeng, L., & Michio, Y. (1996). The onset and interannual variability of the Asian summer monsoon in relation to land sea thermal contrast.American meteorological society, 9, 358—375.

Chi Y, Zhang F, Li W, He J, Guan Z (2015) Correlation between the Onset of the East Asian Subtropical Summer Monsoon and the Eastward Propagation of the Madden–Julian Oscillation, Journal of the Atmospheric Sciences **72**: 1200-1214. DOI: 10.1175/JAS-D-14-0038.1.

Ding Y (2007) The Variability of the Asian Summer Monsoon. *Journal of the Meteorological Society of Japan. Ser. II* **85B**: 21–54. DOI: 10.2151/jmsj.85B.21.

Donald A, Meinke H, Power B, Wheeler M, Ribbe J (2004) Forecasting with the Madden-Julian Oscillation and the applications for risk management, new directions for a diverse planet. The Regional Institute Environment 126: 24-35.

Flohn H (1957) Large-scale Aspects of the “Summer Monsoon” in South and East Asia *Journal of the Meteorological Society of Japan. Ser. II* **35A**: 180–186. DOI: 10.2151/jmsj1923.35A.0_180.

Gelaro R, McCarty W, Suárez M J, Todling R, Molod A, Takacs L, Randles C A, Darmenov A, Bosilovich M G, Reichle R, Wargan K, Coy L, Cullather R, Draper C, Akella S, Buchard V, Conaty A, da Silva A M, Gu W, Kim G, Koster R, Lucchesi R, Merkova D, Nielsen E J, Partyka G, Pawson S, Putman W, Rienecker M, Schubert D S, Sienkiewicz M, Zhao B (2017) The modern-era retrospective analysis for research and applications, version 2 (MERRA-2). *Journal of Climate* **30**: 5419–5454. DOI: 10.1175/JCLI-D-16-0758.1.

Global Modelling and Assimilation Office (2021) The Modern Era Retrospective analysis for Research and Applications, Version 2 (MERRA2). Last access March 2021.

Jones C, Carvalho L (2002) Active and Break phases in the South American Monsoon System. *Journal of Climate*, **15**, 905-914.

Kajikawa Y, Yasunari T, Yoshida S, Fujinami H. 2012. Advanced Asian summer monsoon onset in recent decades. *Geophysical Research Letters* **39:** 1–5. DOI: 10.1029/2011GL050540.

Kanae S, Oki T, Musiake K (2002) Principal condition for the earliest Asian summer monsoon onset. *Geophysical Research Letters* **29**: 34–36. DOI: 10.1029/2002GL015346.

Kiguchi M, Matsumoto J (2005). The Rainfall Phenomena during the Pre-monsoon Period over the Indochina Peninsula in the GAME-IOP Year, 1998. *Journal of the Meteorological Society of Japan. Ser. II*, *83*(1), 89–106. DOI: 10.2151/jmsj.83.89

Kiguchi M, Matsumoto J, Kanae S, Oki T (2016) Pre-Monsoon Rain and Its Relationship with Monsoon Onset over the Indochina Peninsula. In *Frontiers in Earth Science* (**Vol. 4**, p. 42). https://www.frontiersin.org/article/10.3389/feart.2016.00042

Kuraji K, Arthorn B (2011) Rainfall variability over mountainous area in Northern Thailand. JSPS International Forum “Climate Changes in Monsoon Asia” (CCMA), 6-7 Jan. 2011, 45–46.

Li C, Yanai M (1996) The Onset and Interannual Variability of the Asian Summer Monsoon in Relation to Land–Sea Thermal Contrast. *Journal of Climate* **9**: 358–375. DOI: 10.1175/1520-0442(1996)009<0358:TOAIVO>2.0.CO;2.

Madden RA, Julian PR (1971) Detection of a 40–50 Day Oscillation in the Zonal Wind in the Tropical Pacific, Journal of Atmospheric Sciences **28**: 702-708. DOI: 10.1175/1520-0469(1971)028<0702:DOADOI>2.0.CO;2.

Madden RA, Julian PR (1972) Description of Global-Scale Circulation Cells in the Tropics with a 40–50 Day Period*, Journal of Atmospheric Sciences* **29**: 1109-1123. DOI: 10.1175/1520-0469(1972)029<1109:DOGSCC>2.0.CO;2 .

Minoura D, Kawamura R, Matsuura T (2003) A mechanism of the onset of the South Asian summer monsoon. *Journal of the Meteorological Society of Japan* **81**: 563–580. DOI: 10.2151/jmsj.81.563.

Nguyen-Le D, Matsumoto J, Ngo-Duc T (2015) Onset of the Rainy Seasons in the Eastern Indochina Peninsula. *Journal of Climate* **28**: 5645–5666. DOI: 10.1175/JCLI-D-14-00373.1.

Real-time Multivariate MJO indices (2021) RMM Data. Last access 28 June, 2021. http://www.bom.gov.au/climate/mjo/graphics/rmm.74toRealtime.txt

Reynolds RW, Smith TM, Liu C, Chelton DB, Casey KS, Schlax MG (2007) Daily High-Resolution-Blended Analyses for Sea Surface Temperature. *Journal of Climate* **20**: 5473–5496. DOI: 10.1175/2007JCLI1824.1.

Takahashi HG, Yasunari T (2006) A Climatological Monsoon Break in Rainfall over Indochina?A Singularity in the Seasonal March of the Asian Summer Monsoon. *Journal of Climate*, *19*(8), 1545–1556. DOI: 10.1175/JCLI3724.1

Sato T, Kimura F (2007) How does the Tibetan Plateau affect the transition of Indian monsoon rainfall? *Monthly Weather Review* **135**: 2006–2015. DOI: 10.1175/MWR3386.1.

Schumacher C, Ciesielski PE, Zhang MH (2008) Tropical Cloud Heating Profiles: Analysis from KWAJEX, *Monthly Weather Review,* **136**: 4289-4300. DOI: 10.1175/2008MWR2275.1.

Shrivastava S, Kar SC, Sharma AR (2017) Inter-annual variability of summer monsoon rainfall over Myanmar, *International Journal of Climatology, 37(2),* 802-820. DOI: 10.1002/joc.4741.

Tanaka N, Tantasirin C, Aranyabhaga N, Thitirojanawat P, Saphaokham S, Arunpraparut W, Kuraji K (2019) Long-term ecohydrological data at Kog-Ma, Mae Moh and rainfall data at Mae Chaem watershed in northern Thailand. Tokyo: The University of Tokyo Forests Press; p. 125–140.

Taylo CM, Ellis RJ, Parker DJ, Burton RR, Thorncroft CD (2003) Linking boundary-layer variability with convection: A case-study from JET 2000. Quarterly Journal of the Royal Meteorological Society, 129(592), 2233–2253.

The Food and Agriculture Organization (FAO) is a United Nations (UN) (2000) Thailand. http://www.fao.org/3/Y4347E/y4347e1o.htm. Last access June 21, 2021.

The Thai Meteorological Department (TMD) (2021) Climate data chart. https://www.tmd.go.th/en/climate.php?FileID=7. Last access June 21, 2021.

The World Bank (2019) Population, total – Thailand. https://data.worldbank.org/indicator/SP.POP.TOTL?locations=TH. Last access June 21, 2021.

Wang B, Ho L (2002) Rainy season of the Asian-Pacific summer monsson. *Journal of Climate* **15**: 386–398. DOI: 10.1175/1520-0442(2002)015<0386:RSOTAP>2.0.CO;2.

Wang B, Wu R, Lau KM (2001) Interannual Variability of the Asian Summer Monsoon: Contrasts between the Indian and the Western North Pacific–East Asian Monsoons. *Journal of Climate* **14**: 4073–4090. DOI: 10.1175/1520-0442(2001)014<4073:IVOTAS>2.0.CO;2

Wheeler MC, Hendon HH (2004) An all-season real-time multivariate MJO index: Development of anindex for monitoring and prediction. *Monthly Weather Review* **132**: 1917–1932. DOI: 10.1175/1520-0493(2004)132,1917:AARMMI.2.0.CO;2

Wu R, Wang B (2000) Interannual Variability of Summer Monsoon Onset over the Western North Pacific and the Underlying Processes. *Journal of Climate* **13**: 2483–2501. DOI: 10.1175/1520-0442(2000)013<2483:IVOSMO>2.0.CO;2

Xing N, Li J, Wang L (2016) Effect of the early and late onset of summer monsoon over the Bay of Bengal on Asian precipitation in May. *Climate Dynamics* **47**: 1961–1970. DOI: 10.1007/s00382-015-2944-z

Xu J, Chan J CL (2001) First Transition of the Asian Summer Monsoon in 1998 and the Effect of the Tibet-Tropical Indian Ocean Thermal Contrast. *Journal of the Meteorological Society of Japan. Ser. II* **79**: 241–253. DOI: 10.2151/jmsj.79.241

Yanai M, Esbensen S, Chu JH (1973) Determination of Bulk Properties of Tropical Cloud Clusters from Large-Scale Heat and Moisture Budgets. *Journal of Atmospheric Sciences* **30**: 611–627. DOI: 10.1175/1520-0469(1973)030<0611:DOBPOT>2.0.CO;2

Yanai M, Li C, Song Z (1992) Seasonal Heating of the Tibetan Plateau and Its Effects on the Evolution of the Asian Summer Monsoon. *Journal of the Meteorological Society of Japan. Ser. II* **70**: 319–351. DOI: 10.2151/jmsj1965.70.1B_31

Yasutomi N, Hamada A, Yatagai A (2011) Development of a long-term daily gridded temperature dataset and its application to rain/snow iscrimination of daily precipitation. *Global Environmental Research* **15**: 165–172.

Zhang Y, Li T, Wang B, Wu G (2002) Onset of the Summer Monsoon over the Indochina Peninsula: Climatology and Interannual Variations. *Journal of Climate*, *15*(22), 3206–3221. DOI: 10.1175/1520-0442(2002)015<3206:OOTSMO>2.0.CO;2

Zhang Y, Fan G, Hua W, Zhang Y, Wang B, Lai X (2017) Differences in atmospheric heat source between the Tibetan Plateau–South Asia region and the southern Indian Ocean and their impacts on the Indian summer monsoon outbreak. *Journal of Meteorological Research* **31**: 540–554. DOI: 10.1007/s13351-017-6042-5

Zhou ZQ, Xie SP, Zhang R (2019) Variability and Predictability of Indian Rainfall During the Monsoon Onset Month of June. *Geophysical Research Letters***46**: 14782–14788. DOI: 10.1029/2019GL085495

Figures

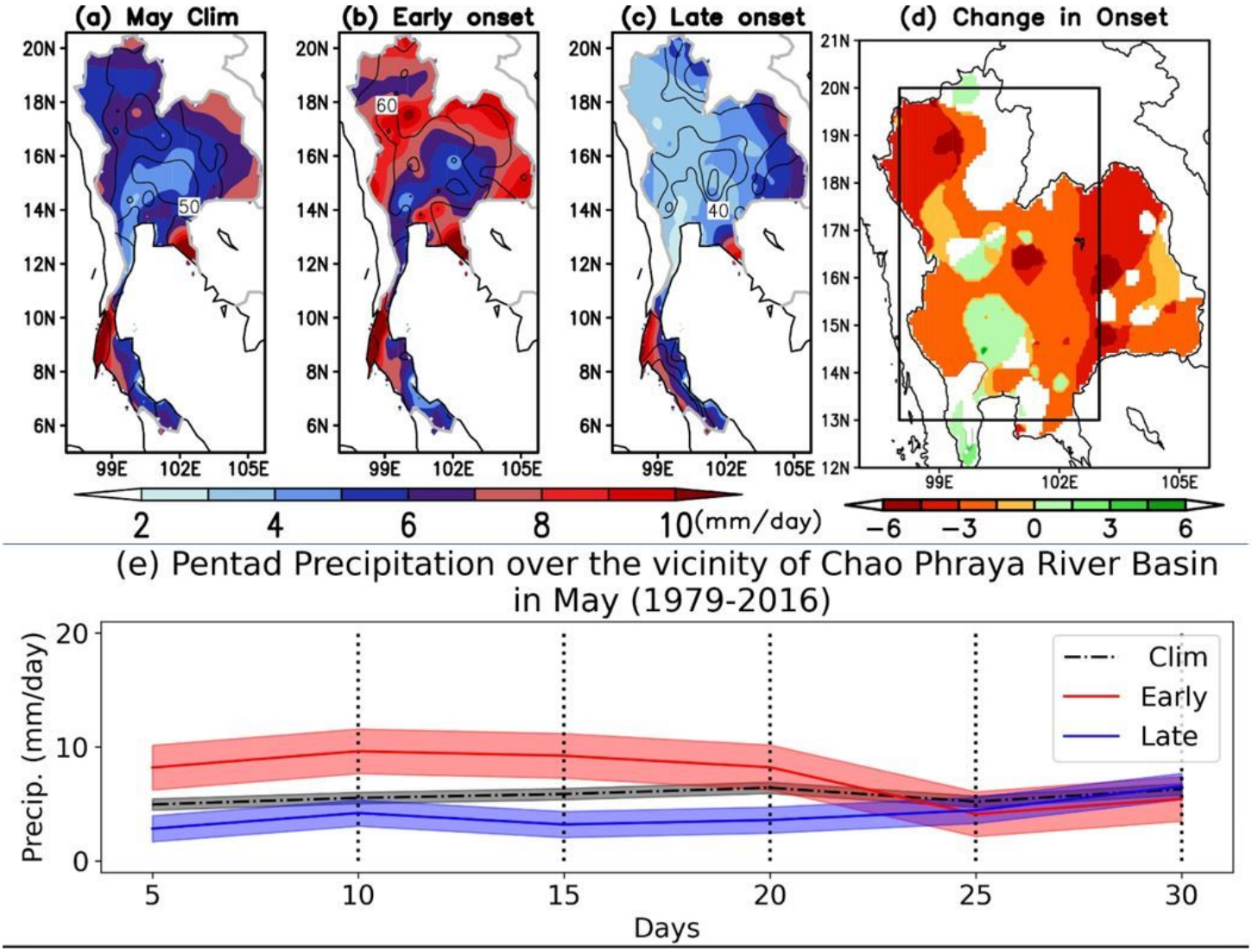

Figure 1

Monthly mean rainfall climatology (mm/day) over Thailand based on TMD data for the period of 1981–2016 for May (a) climatology, (b) early years, and (c) late years, where the contour represents the percentage of rainfall that occurred in the first 15 days versus the whole month of May; (d) changes in the SAM onset pentads between 1999-2016 and 1981-1998 over each grid of northern Thailand, where the box depicts the area chosen for estimating the mean SAM onset date; (e) pentad mean of climatological rainfall (black line), early onset year rainfall (red line) and late onset year rainfall (blue line) over the Chao Phraya River basin for this study.

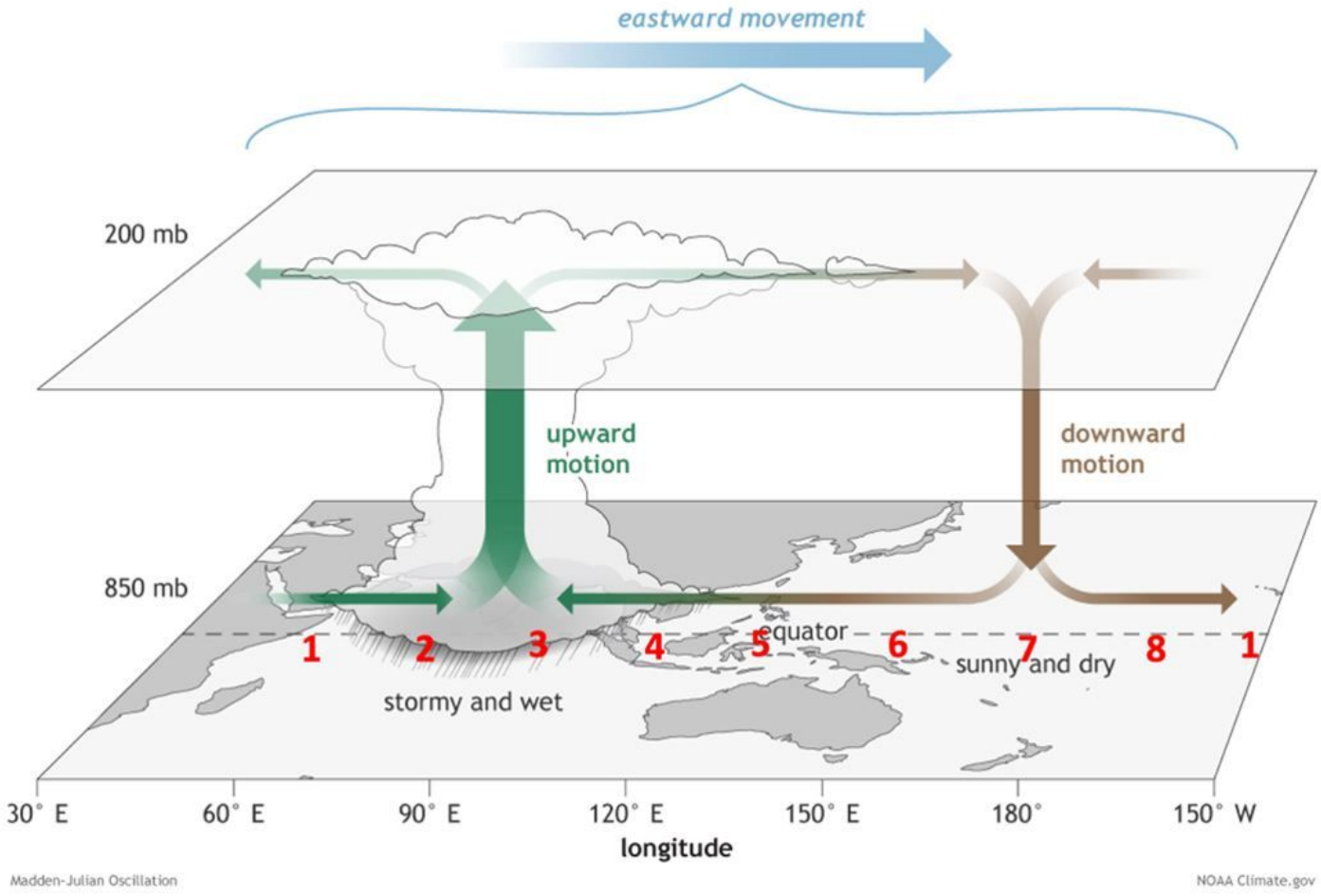

Figure 2

The surface and upper-atmosphere structure of the MJO for a period when the enhanced convective phase (thunderstorm cloud) is centered across the Indian Ocean and the suppressed convective phase is centered over the west-central Pacific Ocean. Horizontal arrows pointing left represent wind departures from average that are easterly, and arrows pointing right represent wind departures from average that are westerly. The entire system shifts eastward over time, eventually circling the globe and returning to its point of origin. Credit: Climate.gov drawing by Fiona Martin. The numbers (RMM Index phases 1-8) in red are the approximate locations of the MJO center of convection. Phase 1 includes signals from both the initiation of an MJO event in the western Indian Ocean basin and the breakdown of MJO events in the mid-Pacific Ocean.

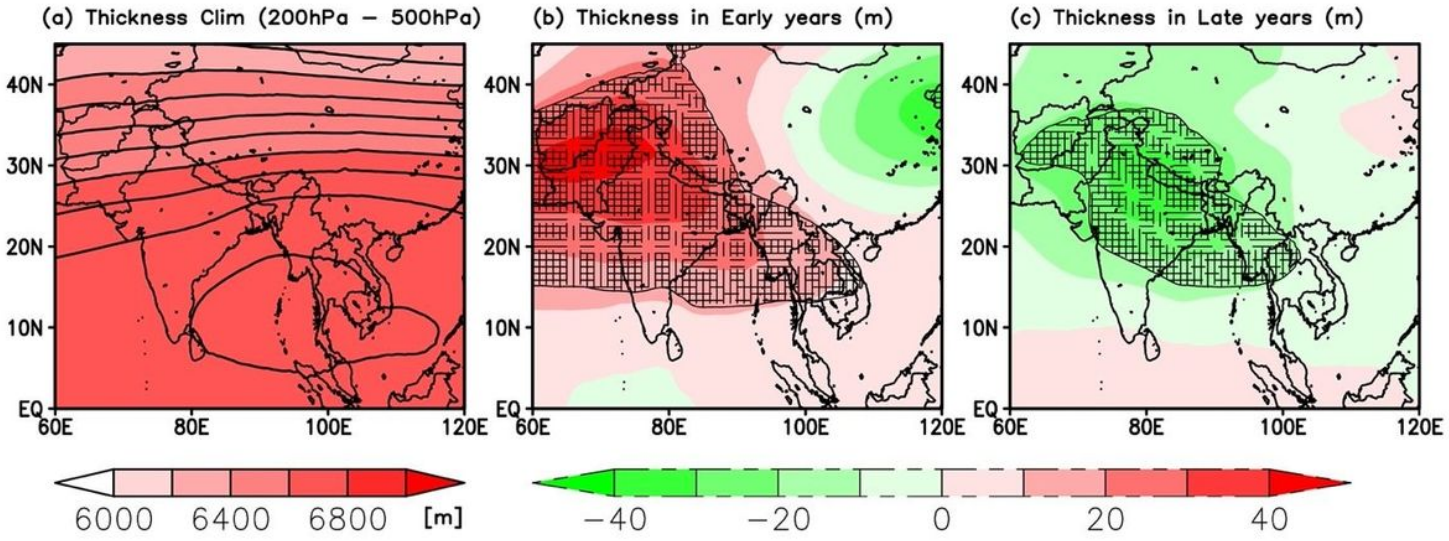

Figure 3

Thickness (p) is the height between 200 hPa minus 500 hPa in meters. a) Climatology of thickness, b) anomalies of thickness for early SAM onset years and c) anomalies of thickness for late SAM onset years. In Figure a, black lines are the contour interval of thickness corresponding to the increasing color. In Figures b and c, the area covered with contours (vertical lines) exceeds the 90% and (horizontal lines) 95% levels of confidence using a two-tailed t test.

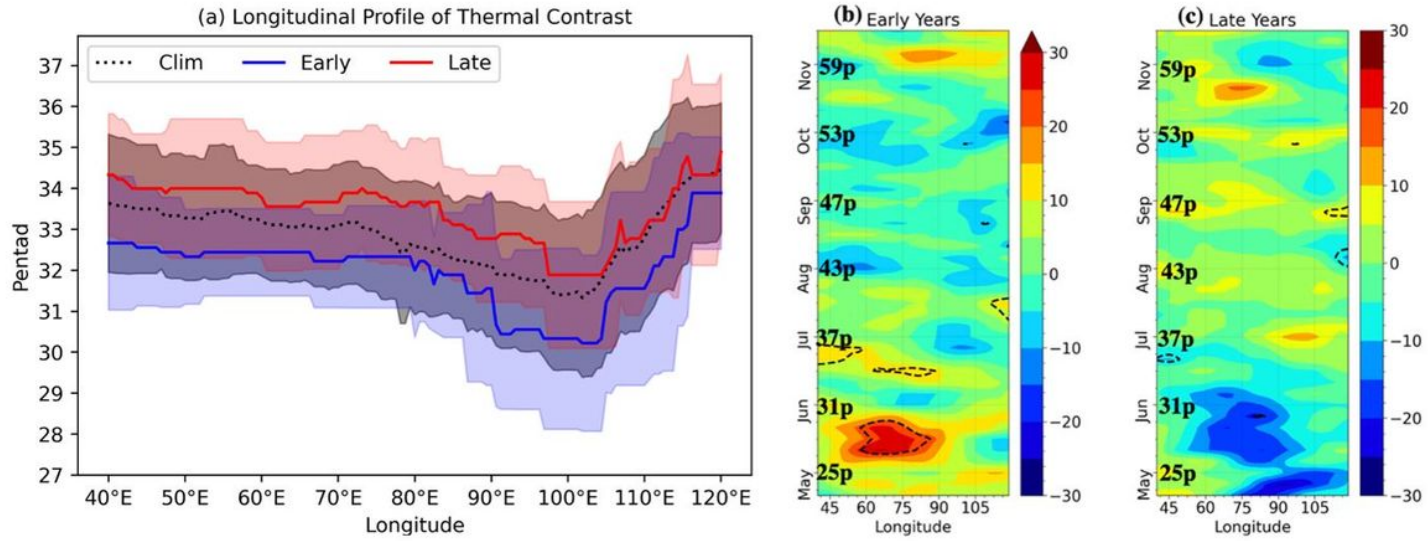

Figure 4

(a) Longitudinal profile of the thermal heat contrast between land and ocean. The black dotted line indicates the climatological average of the pentad of the year when the thermal contrast is zero. Same as the black dotted line but the blue and red solid lines are for the early and late years. In both early and late years, ranges with lighter colors indicate values of year-to-year variability; (b) difference in the thermal

contrast between early years and climatology; right: same as the first panel but for late years for each pentad from January to July. (**p** denotes the pentad for the corresponding month).

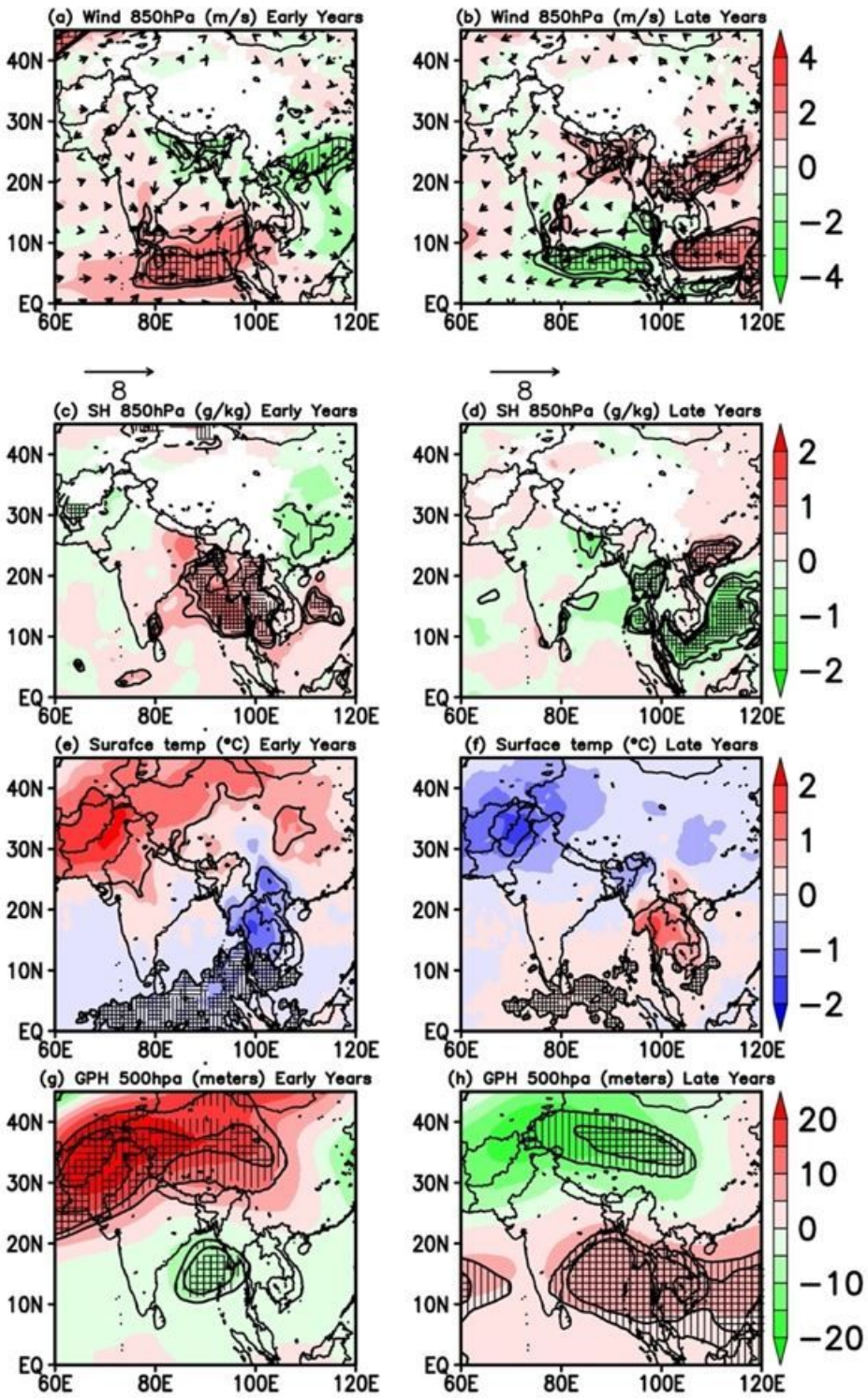

Figure 5

Early and late onset year anomalies during 1981 to 2016 for (a-b) wind at 850 hPa (the color shows the anomaly of wind speed in meters/second), where red is more than and green is less than the climatology.

(c-d) Specific humidity (SH) at 850 hp (the color shows the amount of humidity anomalies in grams/kilogram), where red color is an excess and green is a deficit in SH compared to climatology. (e-f) Surface temperature (ST) over land and ocean (the color shows the ST in degrees Celsius), where red is warmer and blue is cooler STs than climatology. (g-h) Geopotential height at 500 hPa (GPH) (the color shows the GPH in meters), where red is thicker and green is thinner GPH than climatology. The blank area represents undefined values or no data. The area covered with contours (vertical lines) exceeded the 90% and (horizontal lines) 95% levels of confidence using a two-tailed t test.

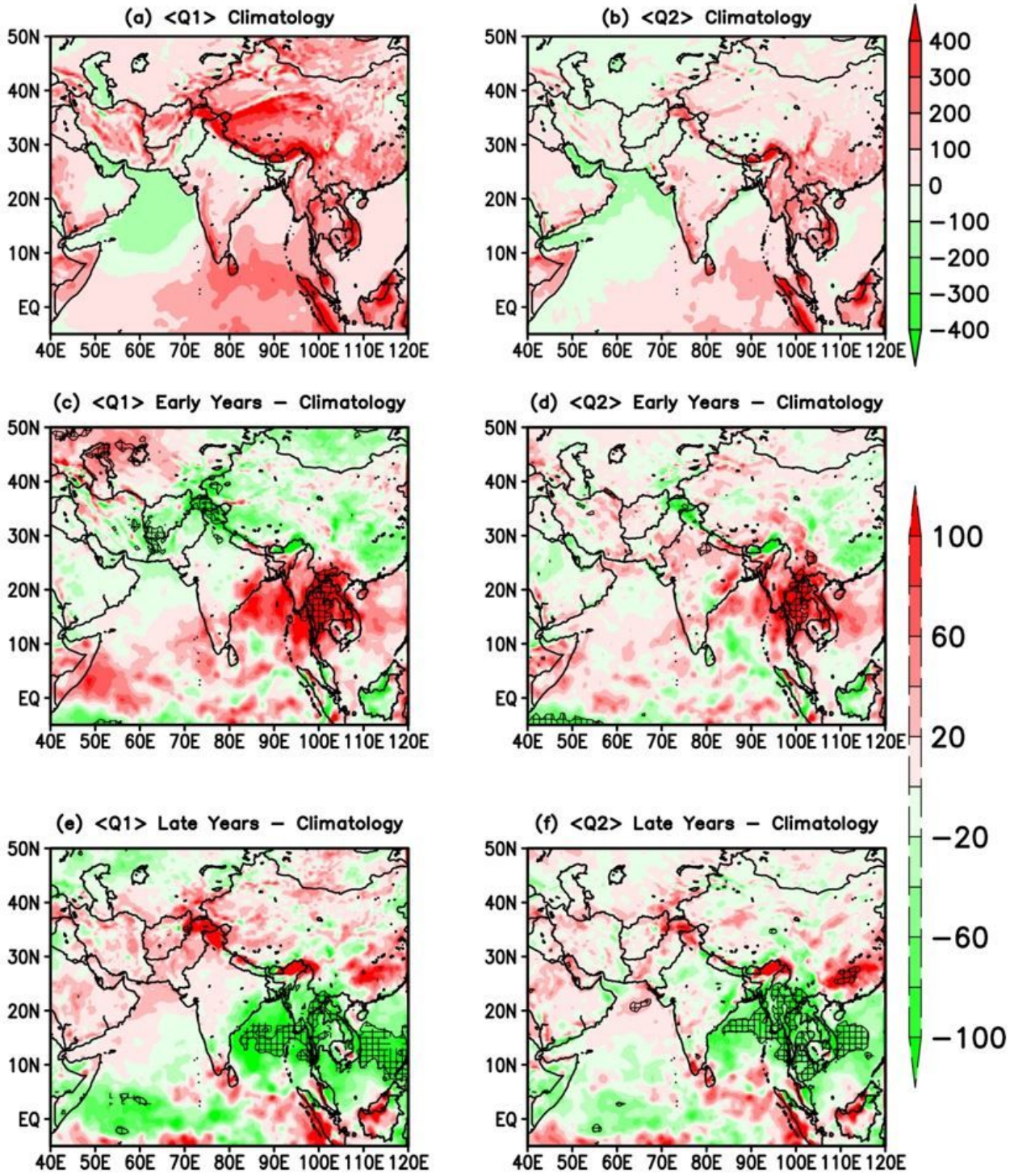

Figure 6

Climatology of a) the vertically integrated apparent heat source (<Q1> W m^{-2}) and b) vertically integrated apparent moisture sink (<Q2> W m^{-2}), anomalies of <Q1> and <Q2> W m^{-2} € for the <Q1> early onset year anomaly, (d) <Q2> early onset year anomaly, (e) for the <Q1> early onset year anomaly and (d) <Q2> late onset year anomaly. The area covered with contours (vertical lines) exceeded the 90% and (horizontal lines) 95% levels of confidence using a two-tailed t test.

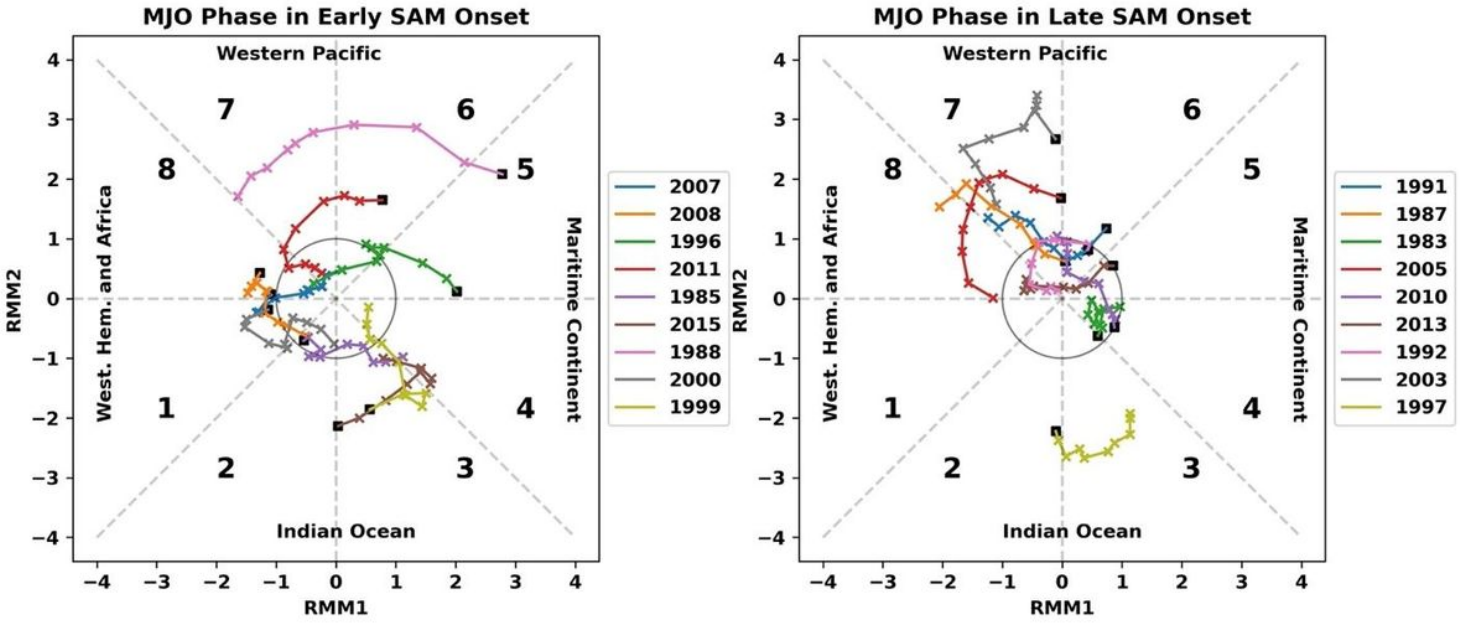

Figure 7

The MJO position and intensity for a) early SAM onset and b) late SAM onset over the CPB. Phase space diagram based on the RMM index of Wheeler and Hendon (2004). Black dots show the location and intensity of the MJO 10 days before SAM onset, and colored lines show the movement and location of the MJO for the last 10 days before onset. MJO = Madden-Julian oscillation; RMM = real-time multivariate MJO index.

Supplementary Files

This is a list of supplementary files associated with this preprint. Click to download.

- Supplimentmat.docx